JACS
JOURNAL OF THE AMERICAN CHEMICAL SOCIETY

COMMUNICATION

pubs.acs.org/JACS

Light Harvesting in Microscale Metal–Organic Frameworks by Energy Migration and Interfacial Electron Transfer Quenching

Caleb A. Kent, Demin Liu, Liqing Ma, John M. Papanikolas, Thomas J. Meyer,* and Wenbin Lin*

Department of Chemistry, CB#3290, University of North Carolina, Chapel Hill, North Carolina 27599, United States

Supporting Information

ABSTRACT: Microscale metal–organic frameworks (MOFs) were synthesized from photoactive Ru(II)-bpy building blocks with strong visible light absorption and long-lived triplet metal-to-ligand charge transfer (^{3}MLCT) excited states. These MOFs underwent efficient luminescence quenching in the presence of either oxidative or reductive quenchers. Up to 98% emission quenching was achieved with either an oxidative quencher (1,4-benzoquinone) or a reductive quencher (*N*,*N*,*N*′,*N*′-tetramethylbenzidine), as a result of rapid energy migration over several hundred nanometers followed by efficient electron transfer quenching at the MOF/solution interface. The photoactive MOFs act as an excellent light-harvesting system by combining intraframework energy migration and interfacial electron transfer quenching.

The chemistry of metal–organic frameworks (MOFs) has evolved rapidly in recent years.[1−4] Most MOF research has focused on storage and separation of small gaseous molecules by taking advantage of their high microporosities.[5−12] However, numerous recent reports have demonstrated that active functional elements can be incorporated into MOFs to create hybrid materials with a range of applications in chemical sensing,[13−16] catalysis,[17−20] biomedical imaging,[21,22] and drug delivery.[23,24] We are interested in utilizing MOFs as active structures for light absorption and excited state applications in energy conversion with the ultimate goal of achieving artificial photosynthesis.

Photosynthesis integrates peripheral, but highly efficient, membrane-bound antenna systems with reaction centers where high yield light-to-redox equivalent conversion is utilized to drive chemical reactions,[25,26] notably water oxidation in Photosystem II[27] and CO_2 reduction in Photosystem I.[28] Chemists have long been interested in developing artificial photosynthetic systems for harvesting and converting sunlight into chemical energy.[29−35] An analogous goal in artificial photosynthesis is integration of light absorption and redox catalysis for solar fuels production.[36] A number of light-harvesting structures have been investigated, including dendrimers,[37] supramolecular structures based on porphyrins, phthalocyanines, perylenebisimides, polypyridyl metal complexes,[38] lanthanide coordination polymers,[39] and bridged semiconducting nanoparticles.[40] Promising results have been obtained on efficient harvesting of photons to give high-energy, redox-separated states.[33]

With their well-defined, repeating structures, functionalized MOFs present an opportunity to design and study dimensionally controlled antenna structures. Ru(II)-bpy derivatized MOFs appear to have promising properties as antennae for sensitizing electron transfer and ultimately, catalytic redox reactions by taking advantage of their ability to absorb light broadly in the visible via metal-to-ligand charge transfer (MLCT) excitations and to undergo facile intracrystal energy transfer. We report successful implementation of this strategy and the first examples of oxidative and reductive interfacial electron transfer quenching of MOF microcrystals (Figure 1a). We demonstrate that Ru(II)-bpy-based MOF microcrystals are highly efficient light-harvesting structures due to their high visible absorptivities, facile intracrystal site-to-site energy migration to the MOF surface, and efficient electron transfer quenching at the MOF/solution interface.

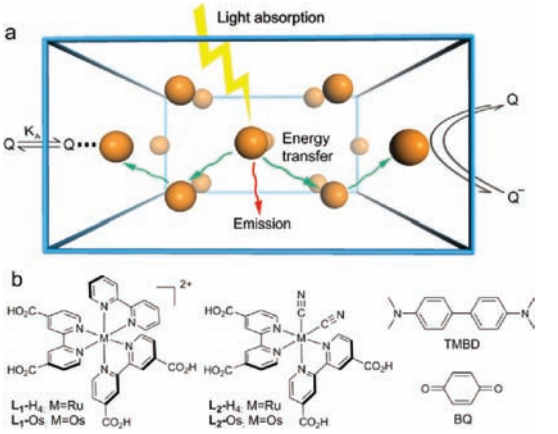

Figure 1. (a) Schematic representation of a light-harvesting MOF microcrystal. The ^{3}MLCT excited states undergo rapid intraframework energy migration to carry out electron transfer quenching at the MOF/solution interface. (b) Chemical structures of the photoactive MOF building blocks and reductive (TMBD) and oxidative (BQ) quenchers.

MOF-**1**, with the formula $[ZnL_1]\cdot 2DMF\cdot 4H_2O$ [where L_1 is $\{Ru[4,4'\text{-}(CO_2)_2\text{-bpy})]_2(bpy)\}^{2-}$], was synthesized as previously reported (DMF is dimethylformamide).[41] MOF-**2**, $[Zn(L_2\text{-}H_2)]\cdot 3H_2O$ [where L_2 is $\{Ru[4,4'\text{-}(CO_2)_2\text{-bpy})]_2(CN)_2\}^{4-}$], was synthesized by a solvothermal reaction between L_2-H_4 and $Zn(NO_3)_2$ in a mixture of water and diethylformamide (DEF). The 2D framework structure of **1** was described previously.[41]

MOF-**2** crystallizes in the orthorhombic space group *Pbcn*, with one L_2–H_2 ligand, one zinc atom, and three water molecules in the asymmetric unit. The Zn center adopts a tetrahedral geometry by coordinating to two carboxylate oxygen atoms of the L_2–H_2 ligands and two nitrogen atoms of the bridging cyano groups. The Zn centers bridge the L_2–H_2 complexes to form 2D pleated sheet structures which pack along the *b* axis with the shortest distance of 6.6 Å between the bpy planes from adjacent

Received: May 17, 2011
Published: July 21, 2011

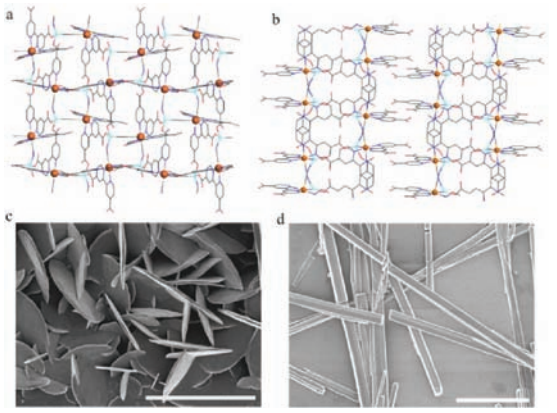

Figure 2. (a) View of 2D structure of MOF-**2**. (b) View of the packing of 2D layers in MOF-**2**. (c) SEM image of disklike microcrystals of **1**. (d) SEM image of rodlike microcrystals of **2**. Scale bars = 5 μm.

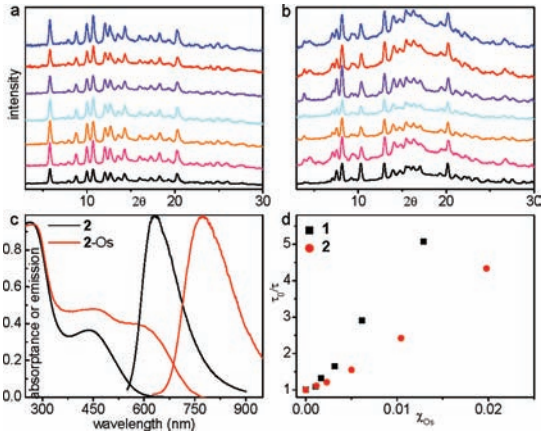

Figure 3. (a) PXRD patterns of microcrystals of **1** with various Os doping levels: the mol % Os (from top to bottom) is 0.0, 0.11, 0.17, 0.32, 0.61, 1.29, and 100. (b) PXRD patterns of microcrystals of **2** with various Os doping levels: the mol % Os (from top to bottom) is 0.0, 0.12, 0.23, 0.50, 1.04, 1.98, and 100. (c) Absorptance and emission spectra of **2** and **2**-Os. (d) Modified Stern–Volmer lifetime analysis of Os-doped MOFs **1** (black squares) and **2** (red circles) by monitoring the Ru(II)* emission at 620 nm (excited at 445 nm).

layers (Figure 2). The shortest intralayer Ru–Ru distance is 6.8 Å, whereas the shortest interlayer Ru–Ru distance is 11.9 Å.

Nano- and microscale MOFs have attracted recent interest due to the potential advantages over bulk phases of MOFs in biomedical and other applications.[21−24] Crystalline microcrystals of **1** and **2** were prepared by modified procedures (Supporting Information [SI]). SEM images showed that disk-shaped particles of **1** were ∼100 nm in thickness and ∼3 μm in diameter (Figure 2c). Needle-like microcrystals of **2** fractured upon drying but were ∼750 nm in diameter and >10 μm in length (Figure 2d). Os complexes $\mathbf{L_1}$-Os and $\mathbf{L_2}$-Os could be doped into microcrystals of **1** and **2**. The mixed Ru/Os MOFs are isomorphous to Ru-only MOFs as shown by PXRD in a and b of Figure 3.

Crystal size plays an important role in light harvesting. The crystal must be able to absorb a high fraction of the incident light but be small enough so that the majority of excited states reach the surface for quenching before excited state decay. The light penetration depths in these MOFs were estimated by application of the Beer–Lambert law. With an effective Ru concentration of 1.5 M calculated from the crystal structure of **2** and a molar absorptivity of 15,000 M cm^{-1}, a ∼150 nm slab can absorb half of the incident light striking the MOF crystal, whereas ∼500 nm is needed to absorb 90% of the incident light (Figure S10 [SI]).

MOF absorptance values were calculated from transmission and reflectance measurements on films of microcrystals held between glass slides. Characteristic ^{1}MLCT absorption bands dominate visible spectra as they do in solution (Figure S12 [SI]). In the **1**-Os and **2**-Os absorption spectra, characteristic low energy S→T MLCT bands appear at 550–750 nm as a result of spin–orbit coupling. Normalized emission spectra of **2** and **2**-Os (Figure 3c), were obtained from degassed, magnetically stirred suspensions of MOF microcrystals in acetonitrile.

The MOF emission decays without added quenchers were satisfactorily fitted with a biexponential expression. Emission decays with added redox quenchers could only be satisfactorily fit to a triexponential decay. The values reported in Table 1 are average lifetimes, calculated by using eq S3b (SI). Average lifetimes are used to phenomenologically describe the system.

A modified Stern–Volmer lifetime analysis was performed on the Os-doped MOFs to determine the relative rates of energy transfer. Direct evidence for energy transfer from Ru(II)* to Os(II) in **1** was demonstrated previously by a delayed growth in the Os(II)* emission.[41] The ratios of the average lifetime of the Ru-only MOF over that of the Os-doped MOF were plotted vs the

Table 1. Absorptance, Emission, and Lifetime Data on Ru and Os MOFs Suspended in Degassed MeCN at 23°C ± 2°C

	abs. λ_{max} (nm)	E_m. λ_{max} (nm)	average lifetime (ns)
1	470	635	610
2	435	630	1100
1-Os	445	765	15
2-Os	450	770	30

mol fraction of Os (Figure 3d). Ru emission lifetime decreases as Os-doping level increases as a result of populating the lower energy Os(II) trap sites via an energy transfer quenching mechanism. As the Os doping levels are quite low in these samples, the Ru(II)* excited states must undergo a number of Ru(II)* → Ru(II) hops before they can encounter an Os(II) trap site. The steeper slope for **1** vs **2** in the τ_0/τ vs χ_{Os} plots in Figure 3d indicate that the rate of energy transfer in **1** is faster than that in **2**.

In order to demonstrate light harvesting, we carried out redox quenching with MOF microcrystals. Interfacial electron transfer quenching experiments were conducted by both emission intensity and lifetime measurements on stirred suspensions of the MOFs in degassed acetonitrile at 23 °C ± 2 °C with added oxidative quencher 1,4-benzoquinone (BQ; $E^{o\prime}$(BQ/BQ$^-$) = −0.52 V vs SCE in acetonitrile with 0.1 M TBAH) or reductive quencher *N*,*N*,*N*′,*N*′-tetramethylbenzidine (TMBD; $E^{o\prime}$(TMBD$^+$) = 0.43 V vs SCE in acetonitrile with 0.1 M TBAH). In these experiments, stock suspensions of the MOFs were pipetted into cuvettes with the quencher subsequently added. The concentrations of MOF were ∼40 μM (based on Ru) as determined by digesting the sample with tetrabutylammonium hydroxide after data collection and measuring the absorbance of the released building blocks.

These data show that the extent of Ru(II)* emission quenching increases as the quencher concentration is increased. With added BQ, greater than 90% quenching of Ru(II)* in **1** is observed at ∼0.3 M while >98% quenching in **2** is obtained at ∼0.1 M BQ. As in solution quenching of related excited states,[42] quenching is by oxidative electron transfer, Ru(II)* + BQ → [Ru(III)]$^+$ + BQ$^{\bullet-}$.

dx.doi.org/10.1021/ja204214t |*J. Am. Chem. Soc.* 2011, 133, 12940–12943

Scheme 1. MOF Emission Quenching with BQ

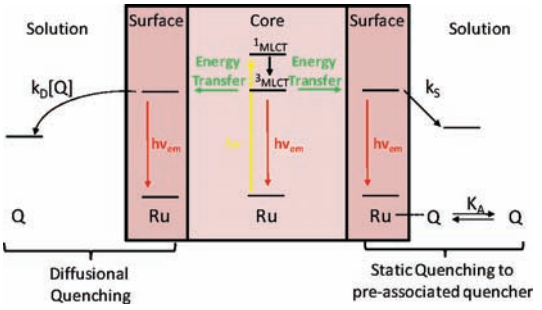

A major contribution from energy transfer is unlikely since the triplet energy of BQ is 18,600 cm^{-1}, ~400 cm^{-1} higher than the lowest MLCT excited state energy in **2**.[43] On the basis of estimated Ru(II)* MOF excited state energies, the driving force for electron transfer is favored by 0.46 eV for **1** and by 0.35 eV by **2**. Preliminary time-resolved electron paramagnetic resonance experiments provided direct evidence for the formation of semihydroquinone free radicals (HBQ•). Irradiation of an ethylene glycol suspension of **2** in the presence of BQ at 500 nm gave $BQ^{\bullet-}$ which subsequently abstracts a proton from trace amount of water in ethylene glycol to yield HBQ•.

Similarly, with added reductive quencher TMBD, 98% of the Ru(II)* emission in **2** was quenched at its solubility limit in MeCN (~20 mM). Quenching of **1** also occurs but much less efficiently. Quenching by TMBD must also have occurred by electron transfer given the absence of a low-lying acceptor excited state for TMBD. Reductive electron transfer quenching by TMBD, Ru(II)* + TMBD → $Ru(II)]^-$ + $TMBD^{+\cdot}$, is favored by 0.74 eV for **1** and by 0.91 eV for **2**.

For quenching of **1** by BQ, the Stern–Volmer plots reveal nearly parallel variations of I_0/I and τ_0/τ with increasing quencher concentration. This behavior is qualitatively consistent with minimal preassociation and/or relatively slow electron transfer with a minor role for static quenching. A significant difference in behavior was observed for **2**. For both oxidative quenching by [BQ] and reductive quenching by [TMBD], plots of I_0/I vs [quencher] are dramatically upward curving while the τ_0/τ data deviate only slightly from linearity. These observations are consistent with preassociation and quenching by both static and dynamic quenching mechanisms. The reversible preassociation of quenchers at the MOF/solution interface of **2** was confirmed by ^{1}H NMR studies on quencher-soaked MOF microcrystals and by the release of TMBD from the MOF microcrystals in fresh solutions as probed by luminescence measurements (SI).

Luminescence quenching behaviors were modeled using the series of reactions depicted in Scheme 1, with quenching by BQ as the example. In the scheme it is assumed that quenching occurs at the MOF/solution interface after migration from the core of the crystal and that there are two quenching pathways. One pathway is diffusional, k_D, while in the other is static, k_S, which involves preassociation at the surface followed by interfacial quenching.

The constants in Scheme 1 and eqs 1 and 2 are: (i) γ: fraction of excited states that reach the MOF/solution interface. τ_0 and τ are the excited state lifetime without and with added quencher, respectively. $\langle\tau\rangle$ is defined in the SI. (ii) K_A: association constant between the quencher and MOF surface. (iii) k_S: rate constant for BQ quenching of Ru(II)* at the surface. (iv) k_D: rate constant for diffusional quenching of Ru(II)* at the MOF/solution interface.

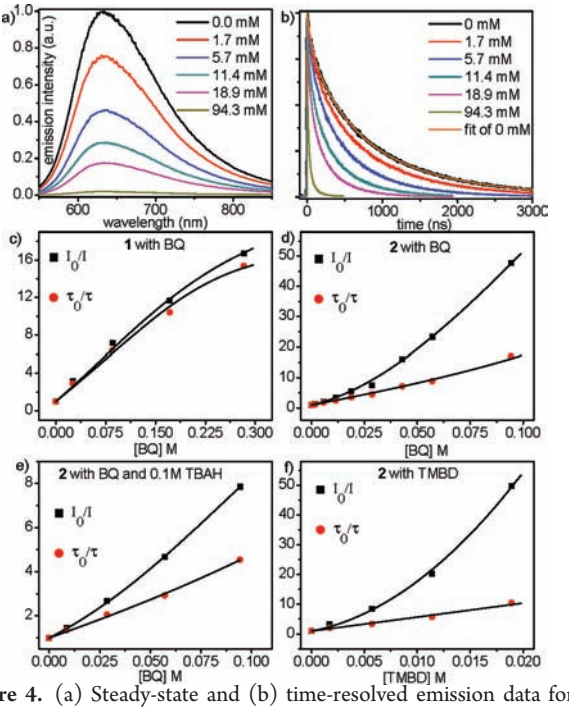

Figure 4. (a) Steady-state and (b) time-resolved emission data for **2** with added BQ in degassed MeCN at 23 °C ± 2 °C. For a Stern–Volmer analysis of steady-state emission, emission intensity was integrated from 550 to 850. Lifetime data were obtained following 485 nm excitation with monitoring at the emission max at 620 nm. Transient decays were fit to the triexponential expression in eq 1, i = 3. (c–f) Steady-state and time-resolved Stern–Volmer quenching analysis of **1** or **2** with BQ or TMBD. Quenching by BQ of (a) **1** (b) **2** (c) **2** with 0.1 M TBAH and (d) quenching of **2** by TMBD.

Table 2. Fitting Results of Stern–Volmer Plots in MeCN

	K_A (M^{-1})	γ	k_S (ns^{-1})	k_D (10^7 M^{-1} s^{-1})
1 - BQ	1.9 ± 1.5	0.9996 ± 0.0002	0.0246 ± 0.005	9.5 ± 0.9
2 - BQ	35.1 ± 3.4	1.000	0.230 ± 0.052	11.4 ± 0.6
2 - BQ, TBAH	13.7 ± 1.8	0.9992 ± 0.0014	0.0265 ± 0.006	2.9 ± 0.2
2 - TMBD	259 ± 31	1.000	>15	34.4 ± 4.4

Equation 1 was derived to describe the steady state Stern–Volmer results (I_0/I vs [quencher]) based on the model in Scheme 1 with $(1 - \gamma)$ being the fraction of excited states that remain in the core of the crystal and are inaccessible to quencher, and $k_{Ru^*}^{-1} = \tau_0$ (SI). Equation 2 was derived to describe the time-resolved Stern–Volmer behavior (τ_0/τ vs [quencher]) (SI). The steady-state and time-resolved Stern–Volmer equations (eqs 1 and 2) were simultaneously fit to the experimental Stern–Volmer plots as shown in Figure 4c–f by application of a nonlinear least-squares regression analysis to extract values for the four adjustable parameters: K_A, γ, k_S, and k_D.

$$\frac{I_0}{I} = \left((1-\gamma) + \gamma F_{SQ} \frac{k_{Ru^*}}{k_{Ru^*} + k_S} + \gamma(1-F_{SQ}) \frac{k_{Ru^*}}{k_{Ru^*} + k_D[Q]} \right)^{-1} \quad (1)$$

$$\frac{\tau_0}{\tau} = \frac{1}{k_{Ru^*}\langle\tau\rangle} \quad (2)$$

Table 2 summarises the fitting results for the Stern–Volmer analysis for BQ and TMBD quenching of **1** and **2**. The solid lines in Figure 4c–f illustrate fits to eqs 1 and 2. For oxidative quenching of **1** by BQ the results of the kinetic analysis are consistent with a small preassociation constant ($K_A = 1.9\ M^{-1}$), high fraction of excited states captured at the interface ($\gamma > 0.99$), and relatively slow electron transfer quenching with $k_S = 2.5 \times 10^7\ s^{-1}$ and $k_D = 9.5 \times 10^7\ M^{-1}\ s^{-1}$. Dual channels for quenching may have a microscopic origin in multiple quenching sites at the crystal/solution interface or may be due to quenching at different faces of the crystal. For quenching of **2** by BQ, $K_A = 35\ M^{-1}$, $\gamma \approx 1$, $k_S = 2.3 \times 10^8\ s^{-1}$; and $k_D = 1.1 \times 10^8\ M^{-1}\ s^{-1}$. A role for the surface interaction in **2** is supported by less efficient quenching with added electrolyte. With 0.1 M added tetrabutylammonium hexafluorophosphate (TBAH), $K_A = 14\ M^{-1}$, $\gamma \approx 1$, $k_S = 2.6 \times 10^7\ s^{-1}$; and $k_D = 2.9 \times 10^7\ M^{-1}\ s^{-1}$.

We have synthesized microscale MOFs based on photoactive Ru(II)-bpy building blocks which show "antenna"-like behaviors with high electron transfer efficiencies (>98%) toward both oxidative and reductive quenching. Efficient electron transfer quenching results from rapid energy migration over several hundred nanometers followed by efficient electron transfer quenching at the MOF/solution interface. Our work is significant in demonstrating MOFs as a viable approach to light harvesting coupled with energy conversion by excited state quenching and electron transfer. Addition of catalytic components to light-harvesting MOFs may lead to novel hybrid materials for efficient artificial photosynthesis and is currently being pursued.

■ ASSOCIATED CONTENT

Supporting Information. Experimental procedures; characterization data; complete ref 24. This material is available free of charge via the Internet at http://pubs.acs.org.

■ AUTHOR INFORMATION

Corresponding Author
wlin@unc.edu

■ ACKNOWLEDGMENT

We thank Prof. Malcolm Forbes and Dr. Robert Schmidt for performing preliminary EPR experiments. This material is based upon work supported as part of the UNC EFRC: Solar Fuels and Next Generation Photovoltaics, an Energy Frontier Research Center funded by the U.S. Department of Energy, Office of Science, Office of Basic Energy Sciences under Award Number DE-SC0001011 (characterization and photophysical studies). C.A.K. and L.M. were partially supported by a NSF Grant to (DMR-0906662) to W.L. (synthesis). C.A.K. was a Carolina Energy Fellow.

■ REFERENCES

(1) Ockwig, N. W.; Delgado-Friedrichs, O.; O'Keeffe, M.; Yaghi, O. M. *Acc. Chem. Res.* **2005**, *38*, 176.
(2) Bradshaw, D.; Warren, J. E.; Rosseinsky, M. J. *Science* **2007**, *315*, 977.
(3) Evans, O. R.; Lin, W. *Acc. Chem. Res.* **2002**, *35*, 511.
(4) Farha, O. K.; Hupp, J. T. *Acc. Chem. Res.* **2010**, *43*, 1166.
(5) Rowsell, J. L.; Yaghi, O. M. *Angew. Chem., Int. Ed.* **2005**, *44*, 4670.
(6) Kesanli, B.; Cui, Y.; Smith, M. R.; Bittner, E. W.; Bockrath, B. C.; Lin, W. B. *Angew. Chem., Int. Ed.* **2005**, *44*, 72.
(7) Dinca, M.; Long, J. R. *Angew. Chem., Int. Ed.* **2008**, *47*, 6766.
(8) Zhao, D.; Yuan, D. Q.; Zhou, H. C. *Energy Environ. Sci.* **2008**, *1*, 222.
(9) Rabone, J.; Yue, Y. F.; Chong, S. Y.; Stylianou, K. C.; Bacsa, J.; Bradshaw, D.; Darling, G. R.; Berry, N. G.; Khimyak, Y. Z.; Ganin, A. Y.; Wiper, P.; Claridge, J. B.; Rosseinsky, M. J. *Science* **2010**, *329*, 1053.
(10) Yang, S.; Lin, X.; Blake, A. J.; Walker, G. S.; Hubberstey, P.; Champness, N. R.; Schroder, M. *Nature Chem.* **2009**, *1*, 487.
(11) Matsuda, R.; Kitaura, R.; Kitagawa, S.; Kubota, Y.; Belosludov, R. V.; Kobayashi, T. C.; Sakamoto, H.; Chiba, T.; Takata, M.; Kawazoe, Y.; Mita, Y. *Nature* **2005**, *436*, 238.
(12) Lee, C. Y.; Bae, Y. S.; Jeong, N. C.; Farha, O. K.; Sarjeant, A. A.; Stern, C. L.; Nickias, P.; Snurr, R. Q.; Hupp, J. T.; Nguyen, S. T. *J. Am. Chem. Soc.* **2011**, *133*, 5228.
(13) Chen, B.; Xiang, S.; Qian, G. *Acc. Chem. Res.* **2010**, *43*, 1115.
(14) Pramanik, S.; Zheng, C.; Zhang, X.; Emge, T. J.; Li, J. *J. Am. Chem. Soc.* **2011**, *133*, 4153.
(15) Allendorf, M. D.; Houk, R. J.; Andruszkiewicz, L.; Talin, A. A.; Pikarsky, J.; Choudhury, A.; Gall, K. A.; Hesketh, P. J. *J. Am. Chem. Soc.* **2008**, *130*, 14404.
(16) Xie, Z.; Ma, L.; deKrafft, K. E.; Jin, A.; Lin, W. *J. Am. Chem. Soc.* **2010**, *132*, 922.
(17) Wu, C. D.; Hu, A.; Zhang, L.; Lin, W. *J. Am. Chem. Soc.* **2005**, *127*, 8940.
(18) Ma, L.; Abney, C.; Lin, W. *Chem. Soc. Rev.* **2009**, *38*, 1248.
(19) Lee, J.; Farha, O. K.; Roberts, J.; Scheidt, K. A.; Nguyen, S. T.; Hupp, J. T. *Chem. Soc. Rev.* **2009**, *38*, 1450.
(20) Ma, L.; Falkowski, J. M.; Abney, C.; Lin, W. *Nature Chem.* **2010**, *2*, 838.
(21) Lin, W.; Rieter, W. J.; Taylor, K. M. *Angew. Chem., Int. Ed.* **2009**, *48*, 650.
(22) deKrafft, K. E.; Xie, Z.; Cao, G.; Tran, S.; Ma, L.; Zhou, O. Z.; Lin, W. *Angew. Chem., Int. Ed.* **2009**, *48*, 9901.
(23) Rieter, W. J.; Pott, K. M.; Taylor, K. M.; Lin, W. *J. Am. Chem. Soc.* **2008**, *130*, 11584.
(24) Horcajada, P.; et al. *Nat. Mater.* **2010**, *9*, 172.
(25) Collini, E.; Wong, C. Y.; Wilk, K. E.; Curmi, P. M. G.; Brumer, P.; Scholes, G. D. *Nature* **2010**, *463*, 644.
(26) Ahn, T. K.; Avenson, T. J.; Ballottari, M.; Cheng, Y. C.; Niyogi, K. K.; Bassi, R.; Fleming, G. R. *Science* **2008**, *320*, 794.
(27) Guskov, A.; Kern, J.; Gabdulkhakov, A.; Broser, M.; Zouni, A.; Saenger, W. *Nat. Struct. Mol. Biol.* **2009**, *16*, 334.
(28) Jordan, P.; Fromme, P.; Witt, H. T.; Klukas, O.; Saenger, W.; Krauss, N. *Nature* **2001**, *411*, 909.
(29) Law, M.; Greene, L. E.; Johnson, J. C.; Saykally, R.; Yang, P. D. *Nat. Mater.* **2005**, *4*, 455.
(30) Concepcion, J. J.; Jurss, J. W.; Brennaman, M. K.; Hoertz, P. G.; Patrocinio, A. O. T.; Murakami Iha, N. Y.; Templeton, J. L.; Meyer, T. J. *Acc. Chem. Res.* **2009**, *42*, 1954.
(31) Gust, D.; Moore, T. A.; Moore, A. L. *Acc. Chem. Res.* **2009**, *42*, 1890.
(32) Morris, A. J.; Meyer, G. J.; Fujita, E. *Acc. Chem. Res.* **2009**, *42*, 1983.
(33) Wasielewski, M. R. *Acc. Chem. Res.* **2009**, *42*, 1910.
(34) Youngblood, W. J.; Lee, S. H. A.; Maeda, K.; Mallouk, T. E. *Acc. Chem. Res.* **2009**, *42*, 1966.
(35) Kelzenberg, M. D.; Boettcher, S. W.; Petykiewicz, J. A.; Turner-Evans, D. B.; Putnam, M. C.; Warren, E. L.; Spurgeon, J. M.; Briggs, R. M.; Lewis, N. S.; Atwater, H. A. *Nat. Mater.* **2010**, *9*, 239.
(36) Hammarstrom, L.; Hammes-Schiffer, S. *Acc. Chem. Res.* **2009**, *42*, 1859.
(37) Wang, J. L.; Yan, J.; Tang, Z. M.; Xiao, Q.; Ma, Y. G.; Pei, J. *J. Am. Chem. Soc.* **2008**, *130*, 9952.
(38) Kobuke, Y. *Eur. J. Inorg. Chem.* **2006**, 2333.
(39) Zhang, X. J.; Ballem, M. A.; Ahren, M.; Suska, A.; Bergman, P.; Uvdal, K. *J. Am. Chem. Soc.* **2010**, *132*, 10391.
(40) Mackowski, S. *J. Phys.: Condens. Matter* **2010**, 22.
(41) Kent, C. A.; Mehl, B. P.; Ma, L. Q.; Papanikolas, J. M.; Meyer, T. J.; Lin, W. B. *J. Am. Chem. Soc.* **2010**, *132*, 12767.
(42) Darwent, J. R.; Kalyanasundaram, K. *J. Chem. Soc., Faraday Trans. II* **1981**, *77*, 373.
(43) Veenvliet, H.; Wiersma, D. A. *Chem. Phys.* **1975**, *8*, 432.